Stochastic Space-Time Downscaling of Rainfall Using Event-Based Multiplicative Cascade Simulations

Bhupendra A. Raut[1,3], Michael J. Reeder[1,2], Christian Jakob[1,2], and Alan W. Seed[4]

[1]School of Earth, Atmosphere and Environment, Monash University, Melbourne, Australia
[2]Australian Research Council Centre of Excellence for Climate Extremes, School of Earth, Atmosphere and Environment, Monash University, Melbourne, Australia
[3]Indian Institute of Tropical Meteorology, Pashan, Pune, India
[4]The Australian Government Bureau of Meteorology, Melbourne, Australia

Key Points:

- A multiplicative cascade model is developed and tested by downscaling ERA-I rainfall.
- Statistical properties of the rainfall at time scales of 6 minutes and spatial scales of 1 km are reproduced.
- Heavy rainfall changes are simulated but with higher uncertainty at higher intensities.

Corresponding author: Bhupendra Raut, bhupendra.raut@monash.edu

Abstract
A multiplicative cascade model called HiDRUS is developed, and tested in the greater Melbourne region (Australia) by downscaling coarse resolution ERA-I rainfall to 1 km horizontal and 6 minute temporal resolutions. The parameters required for the cascade model are computed from radar observations of rain events during 2008–2015, and a library of rainfall events and their associated synoptic conditions created. Each day, the area-averaged rainfall and synoptic conditions are taken from ERA-I and compared with the library. From the library, similar days are chosen randomly and downscaled using the cascade model. Ensembles of 100 realizations per day are produced for the period 1995–2004. The downscaled rainfall is compared with 6-minute rain gauges and daily gridded rain-gauge data at four locations in the greater Melbourne region. HiDRUS reproduces the monthly variability of rainfall, frequency distribution of daily and 6-minute rainfall, and the auto-correlation function satisfactorily. Changes in heavy rainfall are also captured by HiDRUS but with increasing uncertainty as the intensities increase.

1 Introduction

The design criteria for 20^{th} Century urban water infrastructure have mostly been based on historical rain-gauge observations of intensity, duration and frequency of rainfall. However, vulnerabilities of the existing infrastructure have been exposed with rapid urbanization and climate change [*Ashley et al.*, 2005; *Whitehead et al.*, 2009]. As the impact of climate change is realized through changing rainfall, among other things, the resilience of the urban water infrastructure needs to be re-assessed [*Wong and Brown*, 2009; *Arnbjerg-Nielsen et al.*, 2013].

Current General Circulation Models (GCMs) make climate change projections for the 21^{st} Century at relatively coarse space-time resolutions, typically around 100 km and several hours. Such a resolution is unsuitable for the assessment of climate change on urban water infrastructure due to the fast hydrological response to rainfall, particularly in urban catchments, and due to the high space-time variability of rainfall [*Cristiano et al.*, 2017]. Therefore, to better meet the needs of urban water infrastructure design and the assessment of climate change impacts, among other things, rainfall downscaling methods have been devised to generate fine-scale details from the large-scale predictions [*Kim et al.*, 1984; *Willems et al.*, 2012]. Detailed reviews of these downscaling methods can be found in *Wilby and Wigley* [1997]; *Fowler et al.* [2007]; *Benestad et al.* [2008]; *Ekström et al.* [2015].

Downscaling methods fall in two main groups: dynamical downscaling and empirical downscaling. In dynamical downscaling, a regional climate model (RCM) is run at a higher resolution than a GCM (typically by the factor of 3–5) over a limited area and driven by boundary conditions from the coarser-resolution GCM. Multiple nested domains are often used to achieve progressively finer horizontal resolution. Dynamical downscaling is sometimes thought to be better for climate change studies than empirical downscaling as the models explicitly represent the local physical processes. However, physical processes at small (cumulus) scales are not accurately represented in RCMs and consequently the models do not produce realistic sub-hourly time series of rainfall. In that respect, RCMs suffer from similar problems to GCMs, and they inherit the errors of their parent GCM through the boundary conditions [*Mitchell and Hulme*, 1999]. Moreover, dynamical models are computationally expensive, which limits the length of the simulations and size of ensemble.

Empirical models are fundamentally statistical and assume stationarity. The approaches to empirical downscaling can be broadly categorized as follows.

1. Analogue methods assign past events to similar future events. It is a non-linear and non-parametric approach that correctly represents the spatial variability [*Zorita and Von Storch*, 1999]. Due to the rarity of extreme events, however, they are reassigned

several times for long term simulations. This method is limited by the length of the available dataset [*Timbal et al.*, 2003].

2. Regression methods assume that there is a relationship between the large-scale state of the atmosphere and the small-scale state that can be linear or non-linear [*von Storch et al.*, 1993]. These methods have worked well with temperature [*Goyal and Ojha*, 2011]. However, they have not reproduced the observed variability of rainfall well and have underestimated the magnitude of change in accumulations [*Schoof and Pryor*, 2001].
3. Parametric stochastic models, also known as weather generators (WGs) [*Wilks*, 1999], produce time series of some characteristic of the weather (such as dry and wet days) using Markov chains. Weather generators reproduce the variability of daily rainfall at a single site well. Novel methods are developed to achieve spatial coherency in multisite downscaling [*Srikanthan and Pegram*, 2009; *Steinschneider and Brown*, 2013].
4. Weather Typing is sometimes considered a downscaling method. However, it is almost always used with another downscaling method to refine how the parameters are selected. For example, synoptic weather types have been used to condition the parameters for regression methods and weather generators [*Vrac et al.*, 2007].
5. Multi-fractal space-time models can reproduce the fine-scale hierarchical structure of rainfall through scaling laws. They can generate a realistic space-time evolution of a rainfall field [*Seed et al.*, 1999; *Deidda*, 2000]. However, the spatially identical distributed nature of these models result in flat fields of long-term accumulations [*Raut et al.*, 2018]. Moreover, these models need radar coverage or dense network of rain-gauges [*Rupp et al.*, 2012] to estimate the parameters of the cascade model.

The above empirical downscaling methods are usually applied with one of two objectives in mind: (i) to produce high-resolution time series at a point, or (ii) produce high-resolution spatial information. For urban hydrological purposes, however, a downscaling method should produce textitrealistic space-time structures at the resolution of a kilometer and few minutes in order to fill the resolution gap between meteorological models and hydrological models. Multi-fractal methods are a potential solution as they reproduce fine-scale rainfall patterns using fewer parameters compared to other parametric methods. Multiplicative cascade parameters are usually computed from radar or rain-gauge data, and used to disaggregate rainfall in space and/or time [*Rupp et al.*, 2012]. For downscaling applications, the multiplicative cascade parameters can be conditioned on the GCM predictors to achieve a dependence on the synoptic weather regimes [*Over and Gupta*, 1994; *Raut et al.*, 2012].

Since the mid-1980s there have been investigations of the multi-fractal properties of the rainfall over a wide range of scales and intensities [*Lovejoy and Schertzer*, 1985; *Waymire*, 1985; *Schertzer and Lovejoy*, 1988], and multiplicative random cascades have been theorized to model the scaling behaviour of rainfall fields in space [*Menabde et al.*, 1997; *Deidda et al.*, 1999] and time [*Veneziano et al.*, 1996; *Olsson*, 1998; *Schmitt et al.*, 1998; *Seed et al.*, 2000]. Space-time multiplicative cascades based on space-time scaling of the rainfall were formulated [*Marsan et al.*, 1996; *Venugopal et al.*, 1999; *Deidda*, 2000]. Importantly for the present study, *Seed et al.* [1999] and *Seed* [2003] developed a radar-based nowcasting system, known as the Short-Term Ensemble Prediction System (STEPS), using multiplicative cascades to simulate the horizontal reflectivity field. STEPS also includes a Lagrangian advection model along with a hierarchical autoregressive model of order 2 (AR2) to evolve the rain field in time.

STEPS has been used for nowcasting (up to 90 min) [*Seed et al.*, 2013] and for design storm simulations [*Seed et al.*, 2014]. Recently, *Raut et al.* [2018] reported long simulations of rainfall at a time and space resolution of minutes and a kilometer using STEPS. The model was run with perfect cascade parameters estimated from radar observations for each time step of the simulation. The model reproduced the frequency distributions, the spatial and temporal autocorrelation, and the duration and arrival times of storms for heavy rain simulations in downscaling-like runs. The model also reproduced annual accumulations and frequency distributions when run continuously with 7 years of radar data. Due to its stochastic nature,

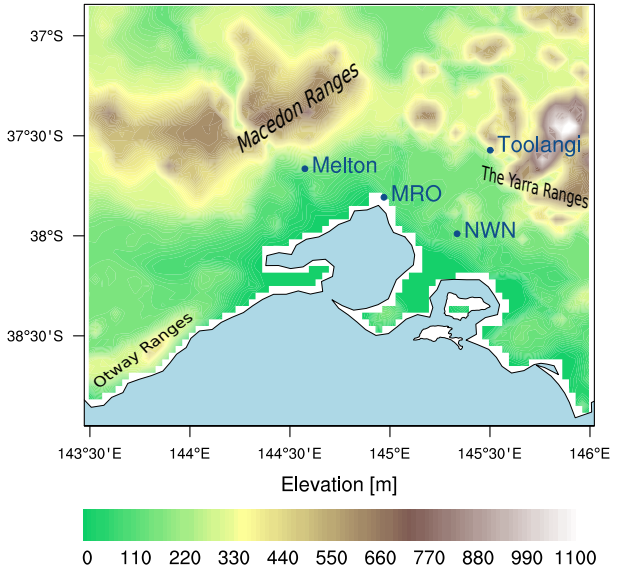

Figure 1. Elevation map for the metropolitan area of Melbourne and surrounding regions. The locations of the 4 sites used to compare the simulated rainfall with the 6-minute rain-gauge data are marked. They are: Melton, Melbourne Regional Office (MRO), Narre Warren North (NWN) and Toolangi. The principal mountain ranges are marked: the Otway Ranges, the Macedon Ranges and the Yarra Ranges.

the model can be run many times with the same parameters to produce an ensemble of simulations. Thus, in principle, STEPS meets the requirements for a high-resolution space-time model that can be used to downscale rainfall if provided the appropriate cascade parameters.

In the current paper, STEPS, as implemented in *Raut et al.* [2018], is used to downscale coarse-resolution ERA-I rainfall data to horizontal and temporal resolutions of 1 km and 6 minutes. The main purpose of the study is to evaluate the feasibility of STEPS as a downscaling model for the future application to GCMs. From this perspective, the ERA-I rainfall is taken to be the best possible model-produced rainfall. The downscaling model developed and used here is called High-resolution Downscaling of Rainfall Using STEPS (HiDRUS) and is outlined in Section 2. Frequency distributions of the downscaled rainfall are compared with observations for the period 1995–2004 in Section 3. Section 4 provides a discussion of the results and summarises the main points of the study.

2 Downscaling Model and Data

2.1 Data

Radar reflectivity data at a 1 km constant altitude plan position indicator for the period 2008–2015 were obtained from Bureau of Meteorology (BoM), Australia. These data are available at 6 minute intervals and at 1 km horizontal resolution over a domain covering 250×250 km centered over Melbourne. Sea Level Pressure (SLP), 10 m horizontal wind vectors and daily precipitation data are taken from the ECMWF Interim reanalysis [ERA-I, *Dee et al.*, 2011]. Rain-gauge observations at 6 minute intervals also come from the BoM and are used to evaluate the downscaled rainfall. Four locations with continuous rain-gauge data in the period 1995–2004 are marked on Figure 1. They are: Melton, Melbourne Regional Office (MRO), Narre Warren North (NWN) and Toolangi. Gridded daily rainfall accumulations at

5 km resolution from the Australian Water Availability Project [AWAP, *Raupach et al.*, 2009; *Jones et al.*, 2009] are also used to evaluate the downscaled daily frequencies of rainfall. All days with more than 0.2 mm of accumulated rain are considered rain days and used in the downscaling.

2.2 Disaggregation Model for Downscaling

A detailed description of STEPS can be found in *Seed et al.* [1999]. In brief, STEPS comprises a set of algorithms to decompose a radar reflectivity field into cascades and to evolve these cascades in time using AR2 models. In nowcasting applications, real-time radar images of the reflectivity are used to estimate a set of cascade parameters; these parameters are the area-mean reflectivity (μ), the spatial variance (σ^2) and the slopes of the power spectrum below and above a predefined scale break (β_1 and β_2 respectively). Advection vectors computed from the radar images translate the cascades in space and the AR2 coefficients evolve the field in Lagrangian coordinates. The field is then normalized by the observed density distribution of reflectivity. Ensemble simulations define the probability of rainfall in the domain.

When applied to nowcasting, the radar reflectivity field also defines the initial structure of the rainfall, after which the cascade parameters are held constant as the rainfall is evolved forward in time. In contrast, when applied to downscaling, the initial realization of the horizontal reflectivity field must be generated before advecting the cascade. The procedure by which the initial realization is generated and evolved is outlined below in Section 2.3.

Due to the identically distributed nature of the cascade generator, STEPS does not produce geographical variations in the long-term rainfall field. For this reason *Raut et al.* [2018] introduced a multiplicative bias correction, defined as ratio of annual-mean rainfall at each point in the domain and the area-mean rainfall. AWAP gridded rain-gauge data for the period 1989–2010 are used to generate the bias correction factors due to the long-term availability and reliability of the data. An explanation of the model setup and bias correction is given in *Raut et al.* [2018].

2.3 HiDRUS Methodology

HiDRUS is the name given to the entire downscaling model and, as illustrated in Figure 2, it has two stages. In the preprocessing stage, the radar reflectivity images are used to compute μ, σ, β_1, β_2 and the mean advection vectors for the field. The first five parameters are domain averages and therefore do not fully describe the reflectivity fields. Therefore, probability distributions of reflectivity fields are are also saved for each time step as suggested in *Raut et al.* [2018].

As part of the preprocessing, a library of rainfall events is constructed. *Rainfall events* are produced by sampling a rainfall time series with a moving window of 24 hours duration (240, 6-minute scans). A rainfall event contains one or more *rainfall episodes* that are defined as at least three consecutive radar scans with the mean area rainfall above 0.1 mm/hr. Figure 3 illustrates the procedure with an example in which 4 rainfall events are generated from 5 rainfall episodes. Episodes 2, 3 and 4 are repeatedly selected and concatenated. The daily-mean rainfall and the synoptic conditions accompanying each rainfall event are also recorded in the library.

Occasionally there may be insufficient radar data to generate extreme daily rainfall events. On these occasions, many events with larger than the observed daily accumulations are generated by connecting two or more adjacent episodes after removing dry periods between them or by repeating the same episode. In this way, the arrival of the storm and its evolution in these synthetically generated events will be realistic. As the time series constructed for one day is independent of the next, a rainfall threshold on the first and the last time-steps is imposed so that instantaneous heavy rainfall does not mark the beginning or end of the day.

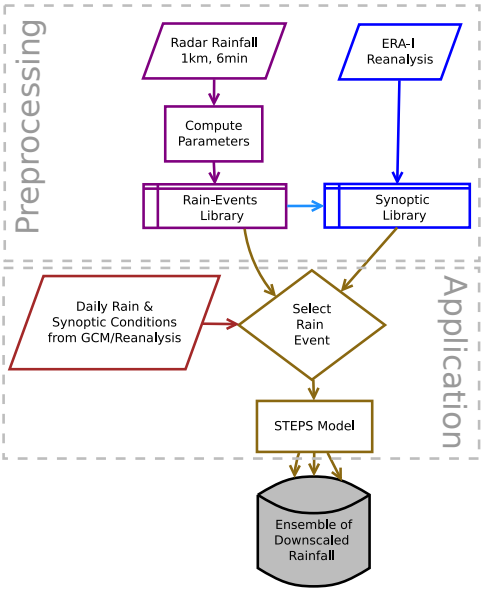

Figure 2. A schematic of the High-resolution Downscaling of Rainfall Using STEPS (HiDRUS) model components and steps.

In the application stage, the ERA-I rainfall is downscaled. For each day, the domain-averaged daily-mean rainfall from ERA-I is calculated and the synoptic conditions identified. These properties are used to match the day with like rainfall events in the library. First events with the matching accumulation of the rainfall are short-listed and then the domain-averaged winds and surface pressure used to select synoptically-similar events, one of which will be selected randomly as the event for that day. Due to the random selection of rainfall events, the ensemble members have different storm structures for the same day.

After selecting parameters for the entire period of simulation (i.e., all the rainy days in the ERA-I), the disaggregation model (STEPS) is invoked to generate space-time downscaling of rainfall at 1 km resolution and 6 min interval. This rainfall disaggregation step works as described in *Raut et al.* [2018]. The second step is repeated 100 times to generate an ensemble of the ERA-I downscaled rainfall. Because of the stochastic nature of the model, individual bursts of rain vary in time and space. Hence, even though the domain-averaged properties of the rainfall are preserved, the individual members of the ERA-I downscaled ensemble have a variety of space-time structures suitable for an investigation of the uncertainty associated with the unpredictable scales of the rainfall processes.

2.4 Comparison of the ERA-I Rainfall with AWAP

In the following section (Section 3), the downscaled ERA-I rainfall from the HiDRUS model is compared with observations from 6-minute rain gauges and AWAP daily gridded rain-gauge data. However, before doing so, the properties of the ERA-I rainfall before downscaling are investigated. Figure 4 compares the area mean ERA-I rainfall (land only) with the AWAP rainfall and the mean of four 6-minute rain gauges.

Although the daily rainfall is underestimated in ERA-I compared to AWAP, their correlation coefficient (CC=0.91) is significant (Figure 4a). It is known that models tend to produce frequent drizzle and less extreme rainfall [*Sun et al.*, 2006]. These model biases are evident from the comparison of frequency histograms shown in Figure 4b. For example, there are 10 events in ERA-I where the mean area accumulation exceeds 20 mm day^{-1} compared with 37

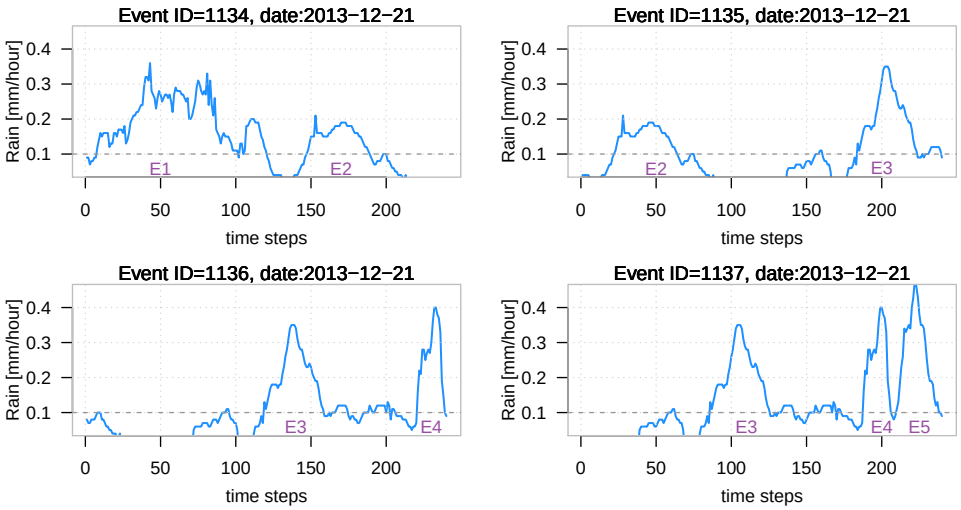

Figure 3. The sampling strategy for the rain library is illustrated with an example. Threshold for a rainfall episode is 0.1 mm/hr. A rainfall episode can be sampled several times to create a large library of events. Four different realisations for the time evolution of the area-average rain rates are shown.

in AWAP. The mean annual rainfall and the 99^{th} percentile are both low for ERA-I rainfall (573 mm, 14 mm respectively) compared to AWAP (760 mm, 19.8 mm, respectively).

Time series of the monthly accumulations in all three data sets (Figure 4c) captures the variability of the rainfall. ERA-I rainfall has a higher correlation with AWAP rainfall (correlation coefficient of 0.93) than with the 6-minute rain-gauge data (correlation coefficient of 0.69). Although the mean of the 6-minute rain gauges need not be representative of area mean rainfall, the downscaled ERA-I rainfall is compared with these rain-gauge observations in Section 3, and it is therefore useful to document the properties of these datasets.

3 Results

This section evaluates the downscaled rainfall ensemble from ERA-I against 6-minute rain-gauge observations at four sites (Melton, Melbourne Regional Office, Narre Warren North and Toolangi) and AWAP daily gridded rain-gauge reanalyses.

3.1 Monthly and Seasonal Rainfall

The monthly-mean downscaled ERA-I rainfall ensemble from the HiDRUS model at the four verification sites are plotted in Figure 5. For comparison, the 6-minute rain-gauge accumulations at each site and their nearest AWAP grid point are also plotted. The differences in the monthly-mean accumulations between the sites are replicated in the downscaled rainfall. Although, the ensemble mean is relatively smooth, individual realizations (gray shaded lines) tend to reproduce the monthly fluctuations well. The sites with higher rainfall, and consequently larger variability, are better represented by the ensemble mean than sites with lower rainfall. Moreover, the correlation coefficients increase from the driest site (Melton) to wettest site (Toolangi) for both AWAP and the 6-minute rain-gauge observations. The correlation between the downscaled ERA-I rainfall with AWAP is 0.42 at Melton and 0.72 at Toolangi, while the correlation with the 6-minute rain-gauge observations increases from 0.31 to 0.60. Like the ERA-I monthly-mean rainfall discussed in Section 2.4 (Figure 4), the ensemble mean of the downscaled ERA-I rainfall is better correlated with AWAP than with the 6-minutes rain gauge observations. Note that the 6-minute rain-gauge observations are point measurements

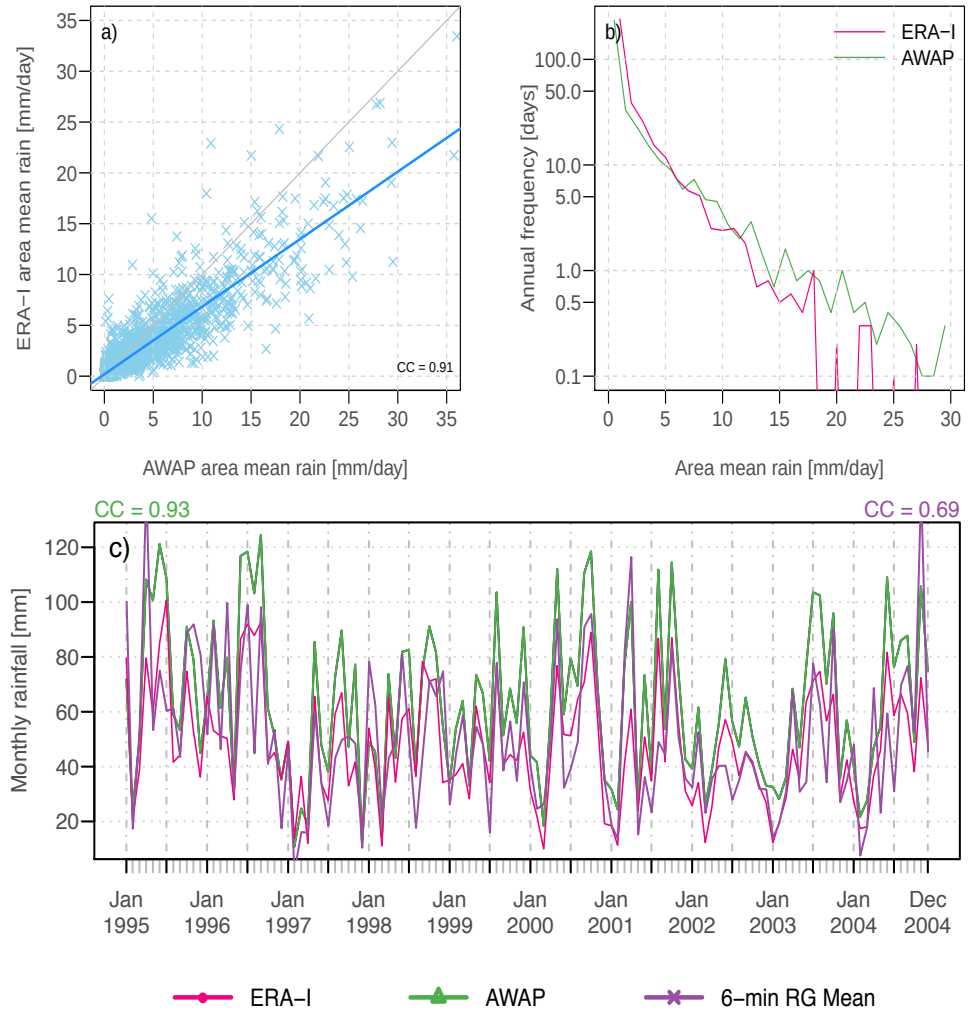

Figure 4. A comparison of the ERA-I rainfall with the AWAP rainfall. a) Domain average ERA-I rainfall (land only) versus AWAP rainfall. b) The frequency distribution of daily rainfall, and c) the monthly-mean rainfall time series for the simulation period. Correlation coefficients of monthly ERA-I rainfall with AWAP and rain gauges are shown at the top of panel c.

whereas AWAP is spatially interpolated. Being spatial simulations, the downscaled ERA-I rainfall compares better to AWAP than to the 6-minute rain-gauge observations. In addition, missing data and under-estimation of heavy rain in the 6-minute rain-gauge observations could be partially responsible for the relatively low correlations.

The annual cycle of monthly-mean rainfall at the four verification sites (Figure 6) has attributes similar to the original-resolution ERA-I rainfall (Figure 4). For example, there is an overestimation of rainfall in AWAP and an underestimation in the 6-minute rain-gauge observations during winter months. The downscaled ERA-I rainfall ensemble has a pronounced seasonal cycle with amplitudes comparable to observations at Narre Warren North and Toolangi. The seasonal variations in the downscaled ERA-I rainfall ensemble closely follow the variations in the observations. However, the downscaled rainfall peaks in winter over Melton and MRO which does not agree well with the observations.

The seasonal-mean rainfall in all the downscaled ensemble members on land is compared to the seasonal-mean of AWAP rainfall in Figure 7. The spatial patterns of rainfall are

well reproduced, with rainfall maxima along the Yarra Ranges to the east of Melbourne, the Macedon Ranges to the north of Melbourne, and the Otway Ranges to the southwest. The rainfall, however, is underestimated in the ensemble mean due mainly to the underestimation of heavy rainfall in ERA-I.

3.2 Frequency Distributions

One aim of downscaling the ERA-I rainfall is to provide realistic frequency distributions of rainfall intensities at finer temporal scales. Figure 8 shows the frequency distributions of the daily-mean rainfall at the four verification sites for the ERA-I downscaled rainfall ensemble, AWAP and the 6-minute rain-gauge accumulations. The frequency distributions of AWAP at the nearest grid points and 6-minute rain-gauge accumulations are consistent at all four verification sites and they fall within the envelop of the downscaled frequency distributions. Over the wetter sites (Toolangi and Narre Warren North) most ensemble members underestimate the frequency of the larger ($>$10 mm) daily accumulations. The spread, and hence uncertainty, within the ensemble increases with the intensity of the rainfall due to fewer occurrences of heavier rainfall.

The frequency distributions at the HiDRUS model's native temporal resolution of 6 minutes are plotted in Figure 9. The frequency distributions for the ERA-I downscaled rainfall ensemble match closely that for the 6-minute rain-gauge accumulations at all sites except Toolangi, which is elevated. At this site the frequency of light rain is over-estimated and the frequency of heavy rain under-estimated more than at the other three sites. Such biases are introduced by the model's underlying assumption that the location of each rainfall event in the domain is random, and it cannot be fixed by a multiplicative bias correction factor. *Raut et al.* [2018] discussed the possibility of the multiplicative cascades, that could be spatially biased to favor genesis in some regions, thereby generating differential frequencies in the events over the domain.

3.3 Autocorrelations

Accurate probabilities of the rain rates is a prerequisite for accurate hydrological models. Moreover, the time structure of the rainfall has a significant impact on the peak flow estimation, especially in urban catchments. With this in mind, the auto-correlation functions for the 6-minute rain-gauge observations and the ERA-I downscaled rainfall ensemble are compared. As shown in Figure 10, the slope of the observed auto-correlation function falls within the ERA-I downscaled rainfall ensemble at all four verification sites. Auto-correlations to a lag of about 18–24 minutes (3–4 time steps) are correctly replicated in the the ERA-I downscaled rainfall ensemble, indicating that the convective-scale evolution of the rain field is well represented. The time taken for the auto-correlations to fall to 0.3 is shortest at Melton (3 time steps) and longest for Toolangi (7 time steps). Narre Warren North and Toolangi rain more than the other sites due to the orography, the effect of which is not included in the cascade model (see *Raut et al.* [2018] for more discussion). Therefore, the auto-correlations in the ERA-I downscaled rainfall ensemble continue to fall at these two locations at a rate faster than that observed. This is a limitation of the HiDRUS model requiring future improvement.

3.4 Heavy Rainfall

A large spread in the ensemble at extreme rain rates is evident from the frequency distributions of the 6-minute rainfall intensity shown earlier in Figure 9. With the increasing resolution of downscaling in space and time, extreme rain rates at a point location are expected to be less robust, and the largest of the values become more uncertain due to stochastic nature of the sampling procedure. Nonetheless, the probabilities of the occurrences of heavy rainfall and their changes in time should be replicated in the ERA-I downscaled rainfall ensemble. The capacity of the HiDRUS model to replicate the occurrence of heavy rainfall and its trend is examined now.

Figure 11 shows the anomalies in 99^{th} and 99.99^{th} percentiles of the hourly-mean rain rates for each year, hereafter called P99 and P99.99 respectively The uncertainty (spread) in the P99 anomaly calculated from the ERA-I downscaled rainfall ensemble is less than the annual variability and the trends are comparable with that of the observations at all sites. The ensemble mean of P99 from the ERA-I downscaled rainfall each year follows that from the 6-minute rain-gauge observations for all sites with a few exceptions, e.g. an over-estimation at Melton. The anomalies of P99.99 rain rates from the ERA-I downscaled rainfall ensemble are noisy and the ensemble means are not variable enough at the drier sites. Nonetheless, the ensemble mean is representative of the heavy rain anomalies over the wetter sites, namely Narre Warren North and Toolangi, albeit with high uncertainty. The annual variability of P99.99 is larger for individual ensemble members than for the observations due to the increasing stochasticity with rainfall rate in the HiDRUS model. Thus, the uncertainty in the prediction of the extreme values of point rainfall is large, as one would expect.

4 Discussion and Conclusions

A multiplicative cascade model, originally developed for nowcasting, is applied to the downscaling for the first time. The ability of the cascade model, called HiDRUS, to reproduce realistic rainfall structures in space and to evolve these structures realistically in time was demonstrated in our earlier work [*Raut et al.*, 2018]. Here this ability is successfully exploited to downscale ERA-I rainfall from spatial and temporal scales of 100 km and daily respectively to 1 km and 6 minutes. Radar data are used to estimate the cascade model parameters for every time step in which there is rain. A library of rainfall events is created with all the parameters and associated synoptic conditions for a given day. During the simulation, events are matched with those from the library based on the domain average rainfall and synoptic conditions on that day. The model is then run with different combinations of matched events to generate 100 realizations of the day. The ERA-I downscaled rainfall is evaluated against AWAP rainfall and 6-minute rain-gauge observations. The downscaled rainfall is shown to reproduce the variability in the monthly-mean accumulations and the seasonal cycle at four verification sites representative of different rainfall conditions in the region. The observed frequency distribution of the daily-mean rainfall and 6-minute rain rates fall within the ensemble spread. The correlation structure of 6-minute rainfall time series at the four verification sites is replicated well by the ERA-I downscaled rainfall ensemble. In addition, anomalies in the probability of heavy rainfall based on the ERA-I downscaled rainfall ensemble are in reasonable agreement with the observations although, of course, the ensemble spread increases as the rain rates increase.

Due to the spatially identical distribution of modeled rain intensity, orographic enhancement and suppression of rainfall is accomplished with a multiplicative bias correction. In *Raut et al.* [2018], simulations made with the cascade model were compared with radar observations, and hence the bias mask used was created from the same radar data. In the present study, the annual-mean gridded rain-gauge observations are used to correct the orographic biases due to their better quality and coverage. The bias correction results in the correct rainfall accumulations at each site while still reproducing the frequency distribution of the rainfall. Moreover, the bias correction does not affect the auto-correlation.

The HiDRUS model captures heavy rainfall, with increasingly large ensemble spread as the rainfall rate increases. The probability of extreme hourly-mean accumulations at a point is not directly a function of the intensity of convective core, but is determined in large measure by stochastic factors such as the organization of convective regions with respect to the location, the propagation speed of the system and the movement of individual convective cells with respect to the large-scale rain field. In this way, successive convective cells pass embedded in a slow-moving system can cause heavy rainfall at a point. The orographic enhancement of rainfall also causes large accumulations at a location. Although the model reproduces the seasonal and interannual variations in heavy rainfall intensities, the trends at higher values are noisy due to the stochastic nature of the processes.

The HiDRUS model will be used to downscale climate model projections for hydrological purposes. As in the downscaling described in the present paper, the time series of the cascade model parameters from actual rainfall events will be used to create realizations of rainfall events. The application of this method to GCM projections is of practical interest to the wider hydrological community. We have performed preliminary studies of the HiDRUS model output using GCMs for evaluating the reliability of stormwater infrastructure as an alternative water supply in Melbourne, Australia [*Zhang et al.*, 2019]. Similar work will be reported on in future studies.

Acknowledgments
This work received funding from Cooperative Research Centre for Water Sensitive Cities (CRC-WSC), Australia and Public Utilities Board (PUB), Singapore. We are thankful to researchers, engineers and policy makers working in the following organizations for their useful feedback during the development of the model: CRC-WSC, Tropical Marine Science Institute, National University of Singapore, PUB-Singapore, and Centre of Climate Research for Singapore (CCRS). The radar data used here can be obtained from the Australian Bureau of Meteorology, and the European Centre for Medium-Range Weather Forecasts. The numerical calculations reported here were done at the National Computational Infrastructure National Facility in Canberra, Australia, which is supported by the Australian Commonwealth Government. The R programming language (http://www.R-project.org), the National Center for Atmospheric Research Command Language (NCL; http://dx.doi.org/10.5065/D6WD3XH5) and Climate Data Operators (CDO) were used in the analysis of the data and in making the graphics. We are grateful to Prof. Geoff Pegram for his insightful comments that improved the original manuscript.

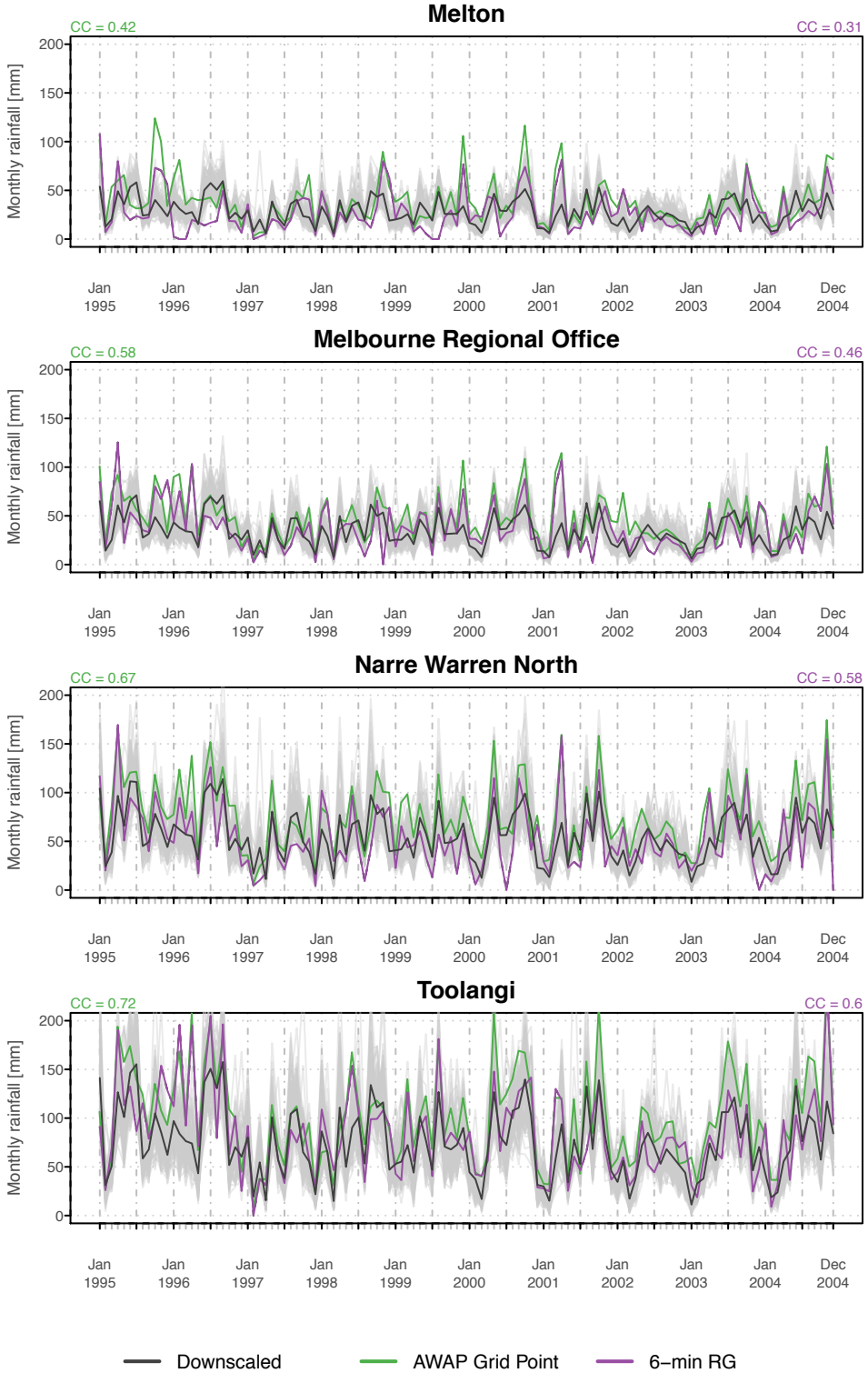

Figure 5. Monthly-mean ERA-I downscaled rainfall at the four verification sites (Melton, Melbourne Regional Office, Narre Warren North and Toolangi) for 100 simulations (gray) and the ensemble mean of downscaled rainfall (dark gray). 6-minute rain-gauge accumulations (purple) and their nearest AWAP grid point (green). Cross-correlations between downscaled data and others are shown at the top of each panel.

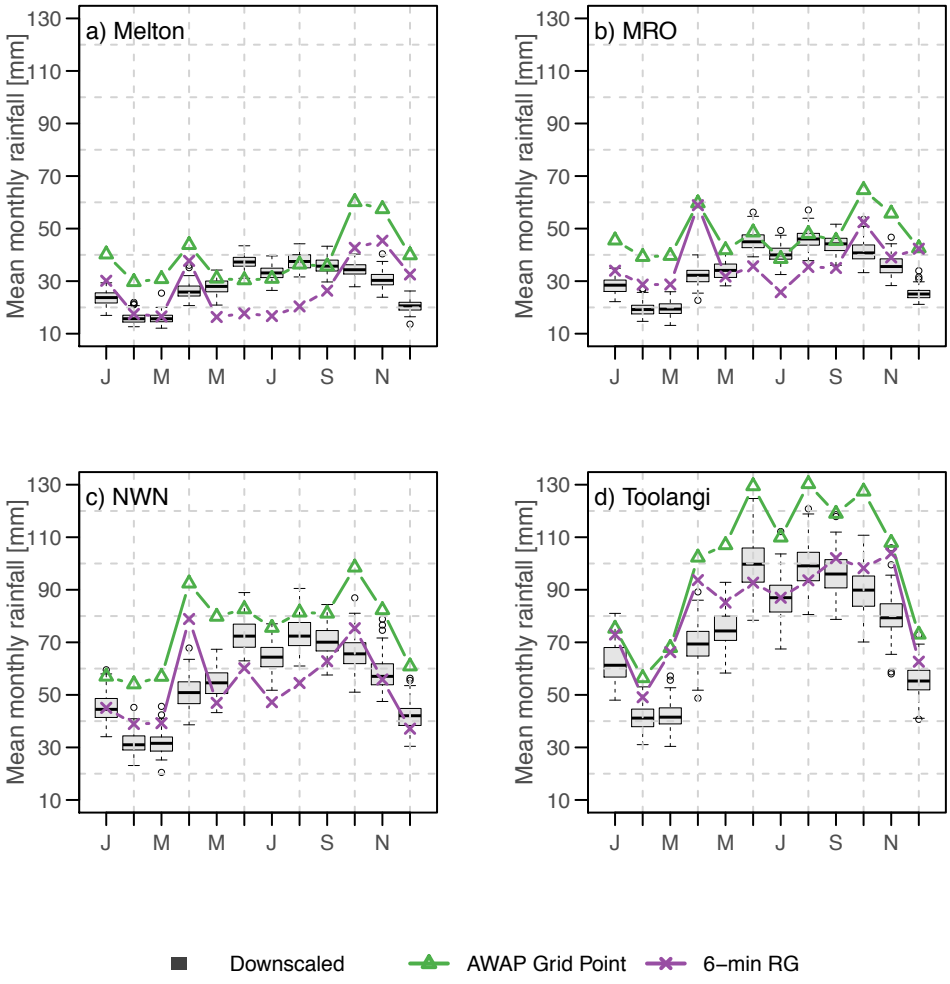

Figure 6. Annual cycle of the monthly-mean ERA-I downscaled rainfall at the four verification sites (Melton, Melbourne Regional Office (MRO), Narre Warren North (NWN) and Toolangi) for 100 simulations (box and whiskers). Annual cycle of the monthly-mean nearest AWAP grid point (green) and the 6-minute rain-gauge accumulations (purple).

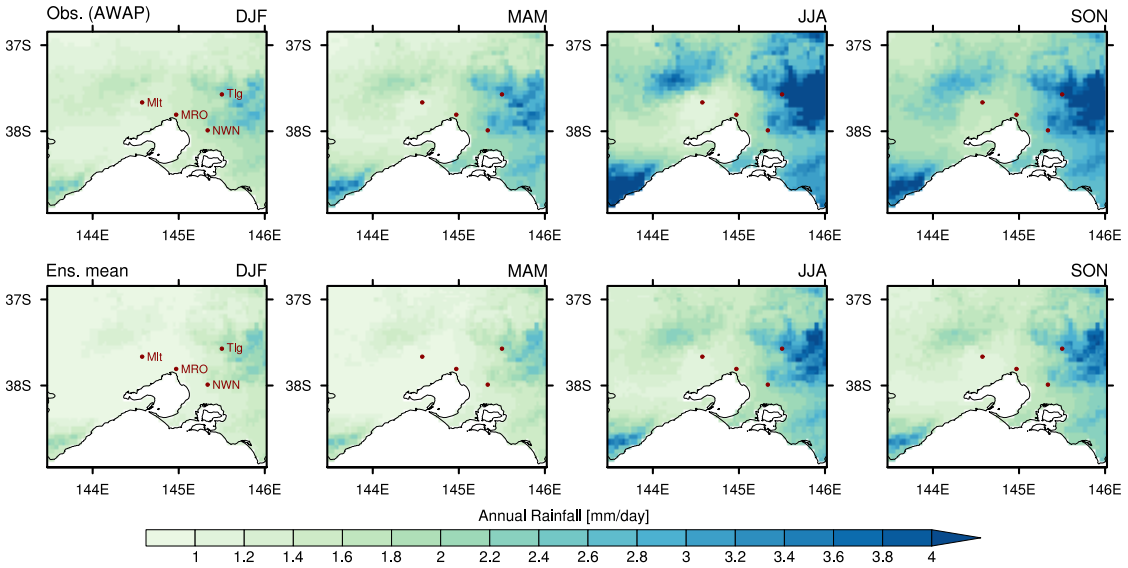

Figure 7. Seasonal-mean rainfall maps (land only) for the period 1995-2004. Top: AWAP. Bottom: ensemble-mean of 100 realizations of downscaled ERA-I rainfall. The four verification sites Melton (Mlt), Melbourne Regional Office (MRO), Narre Warren North (NWN), and Toolangi (Tlg)) are marked.

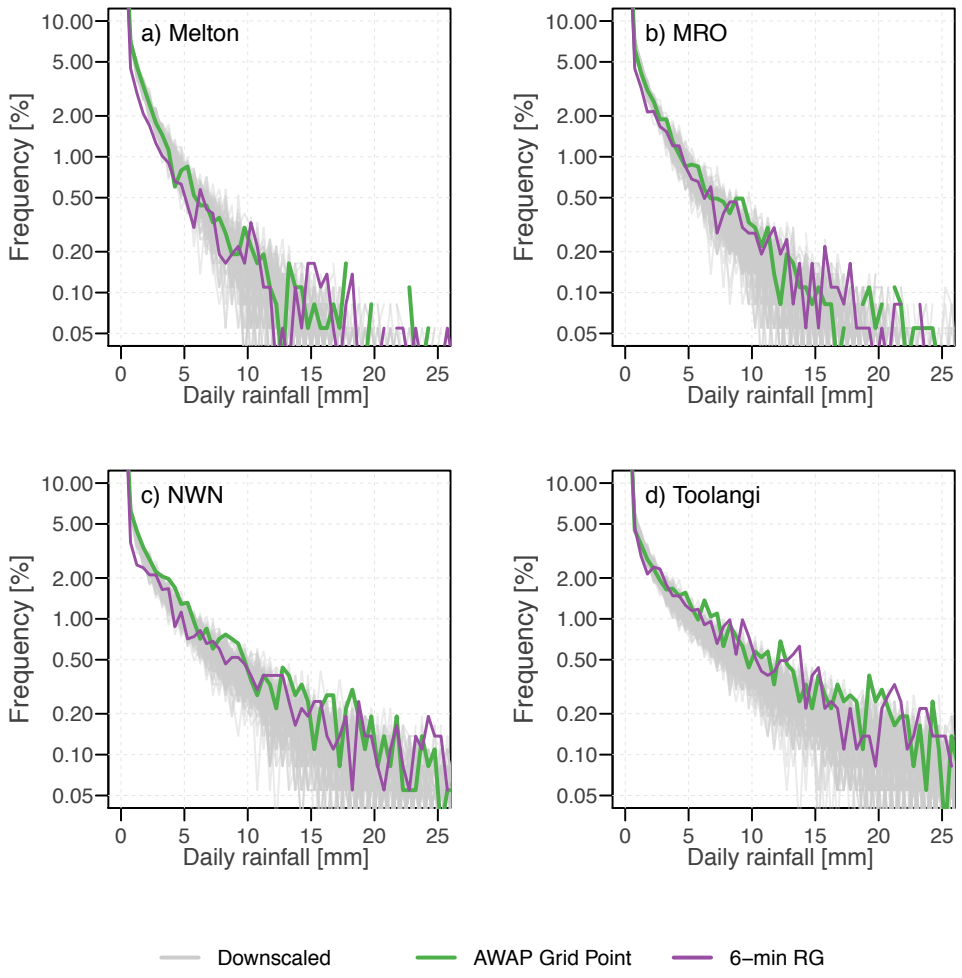

Figure 8. Frequency distribution of the daily-mean rainfall at the four verification sites (Melton, Melbourne Regional Office (MRO), Narre Warren North (NWN). ERA-I downscaled rainfall ensemble (gray), AWAP nearest grid point (green) and 6-minute rain-gauge accumulations (purple).

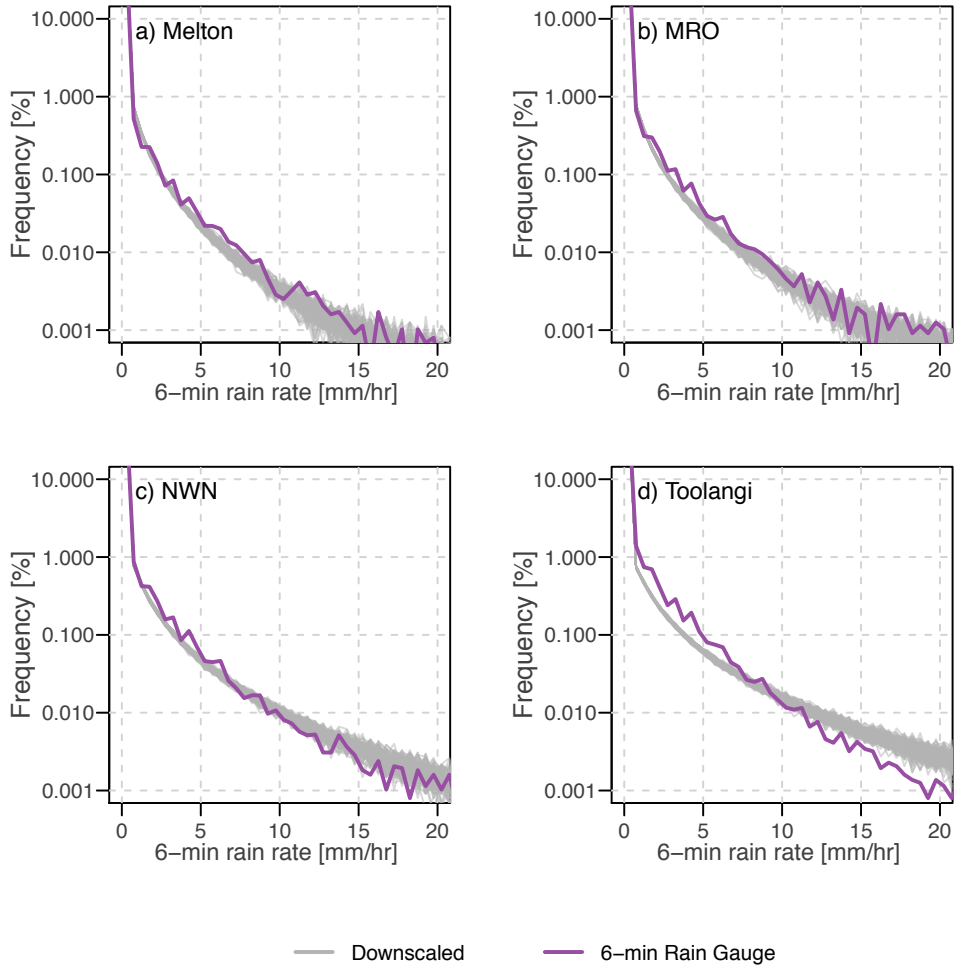

Figure 9. Frequency distribution of the 6-minute rain rates at the four verification sites (Melton, Melbourne Regional Office (MRO), Narre Warren North (NWN). ERA-I downscaled rainfall ensemble (gray) and 6-minute rain-gauge accumulations (purple).

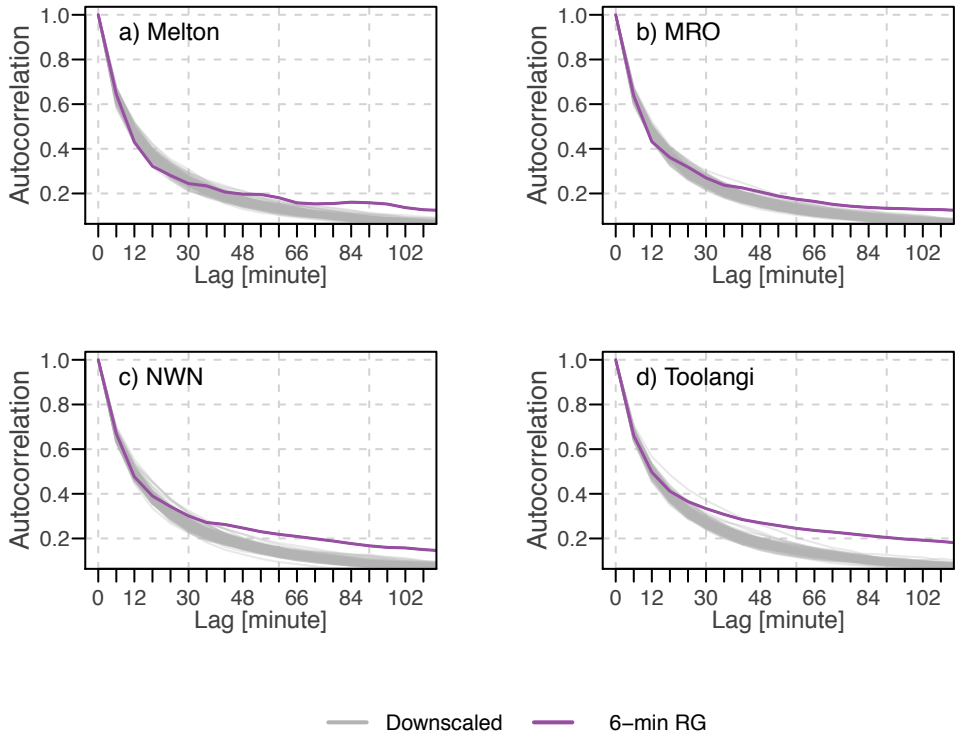

Figure 10. Correlograms of the 6-minute rainfall intensities from the downscaled ERA-I rainfall ensemble and rain gauges at the four verification sites (Melton, Melbourne Regional Office (MRO), Narre Warren North (NWN).

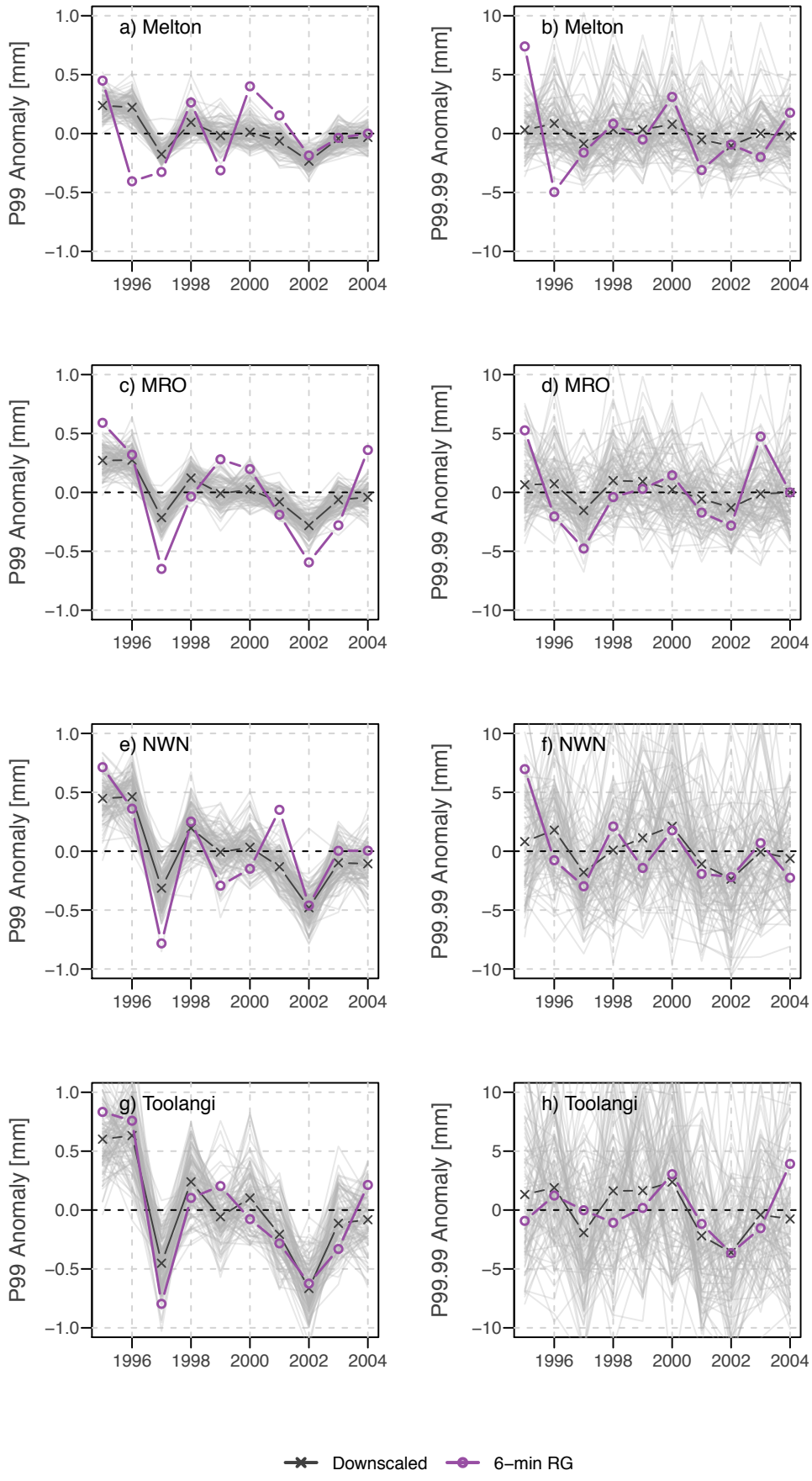

Figure 11. Anomalies in annual 99^{th} (left) and 99.99^{th} (right) percentile of hourly rainfall at the four verification sites (Melton, Melbourne Regional Office (MRO), Narre Warren North (NWN).

References

Arnbjerg-Nielsen, K., P. Willems, J. Olsson, S. Beecham, A. Pathirana, I. B. Gregersen, H. Madsen, and V.-T.-V. Nguyen (2013), Impacts of climate change on rainfall extremes and urban drainage systems: A review, *Wat. Sci. Tech.*, *68*(1), 16–28.

Ashley, R. M., D. J. Balmforth, A. J. Saul, and J. Blanskby (2005), Flooding in the future–predicting climate change, risks and responses in urban areas, *Wat. Sci. Tech.*, *52*(5), 265–273.

Benestad, R. E., I. Hanssen-Bauer, and D. Chen (2008), *Empirical-statistical downscaling*, 214 pp., World Scientific Publishing Company.

Cristiano, E., N. van de Giesen, et al. (2017), Spatial and temporal variability of rainfall and their effects on hydrological response in urban areas–a review, *Hydrol. Earth Syst. Sci.*, *21*(7), 3859.

Dee, D. P., S. Uppala, A. Simmons, P. Berrisford, P. Poli, S. Kobayashi, U. Andrae, M. Balmaseda, G. Balsamo, d. P. Bauer, et al. (2011), The ERA-Interim reanalysis: Configuration and performance of the data assimilation system, *Quart. J. Roy. Meteor. Soc.*, *137*(656), 553–597.

Deidda, R. (2000), Rainfall downscaling in a space-time multifractal framework, *Water Resour. Res.*, *36*(7), 1779–1794.

Deidda, R., R. Benzi, and F. Siccardi (1999), Multifractal modeling of anomalous scaling laws in rainfall, *Water Resour. Res.*, *35*(6), 1853–1867.

Ekström, M., M. R. Grose, and P. H. Whetton (2015), An appraisal of downscaling methods used in climate change research, *Wiley Interdiscip. Rev. Clim. Change*, *6*(3), 301–319.

Fowler, H. J., S. Blenkinsop, and C. Tebaldi (2007), Linking climate change modelling to impacts studies: recent advances in downscaling techniques for hydrological modelling, *Int. J. Climatol.*, *27*(12), 1547–1578.

Goyal, M. K., and C. Ojha (2011), Evaluation of linear regression methods as downscaling tools in temperature projections over the Pichola Lake Basin in India, *Hydrol. Process.*, *25*(9), 1453–1465.

Jones, D. A., W. Wang, and R. Fawcett (2009), High-quality spatial climate data-sets for Australia, *Aust. Meteorol. Ocean.*, *58*(4), 233.

Kim, J., J. Chang, N. Baker, D. Wilks, and W. Gates (1984), The statistical problem of climate inversion: Determination of the relationship between local and large-scale climate, *Mon. Wea. Rev.*, *112*(10), 2069–2077.

Lovejoy, S., and D. Schertzer (1985), Generalized scale invariance in the atmosphere and fractal models of rain, *Water Resour. Res.*, *21*(8), 1233–1250.

Marsan, D., D. Schertzer, and S. Lovejoy (1996), Causal space-time multifractal processes: Predictability and forecasting of rain fields, *J. Geophys. Res.*, *101*(D21), 26,333–26,346.

Menabde, M., D. Harris, A. Seed, G. Austin, and D. Stow (1997), Multiscaling properties of rainfall and bounded random cascades, *Water Resour. Res.*, *33*(12), 2823–2830.

Mitchell, T. D., and M. Hulme (1999), Predicting regional climate change: Living with uncertainty, *Prog. Phys. Geogr.*, *23*(1), 57–78.

Olsson, J. (1998), Evaluation of a scaling cascade model for temporal rain-fall disaggregation, *Hydrol. Earth Syst. Sci.*, *2*(1), 19–30.

Over, T. M., and V. K. Gupta (1994), Statistical analysis of mesoscale rainfall: Dependence of a random cascade generator on large-scale forcing, *J. Appl. Meteor.*, *33*(12), 1526–1542.

Raupach, M., P. Briggs, V. Haverd, E. King, M. Paget, and C. Trudinger (2009), Australian water availability project (AWAP): CSIRO marine and atmospheric research component: final report for phase 3, *Melbourne: Centre for Australian weather and climate research (bureau of meteorology and CSIRO)*, *67*.

Raut, B., L. de la Fuente, A. W. Seed, C. Jakob, and M. J. Reeder (2012), Application of a space-time stochastic model for downscaling future rainfall projections, in *Hydrology and Water Resources Symposium*, pp. 579–586, Engineers Australia.

Raut, B. A., A. W. Seed, M. J. Reeder, and C. Jakob (2018), A multiplicative cascade model for high-resolution space-time downscaling of rainfall, *J. Geophys. Res.*, *123*(4), 2050–2067.

Rupp, D., P. Licznar, W. Adamowski, and M. Lesniewski (2012), Multiplicative cascade models for fine spatial downscaling of rainfall: parameterization with rain gauge data, *Hydrol. Earth Syst. Sci.*, *16*, 671–684.

Schertzer, D., and S. Lovejoy (1988), Multifractal simulations and analysis of clouds by multiplicative processes, *Atmos. Res.*, *21*(3-4), 337–361.

Schmitt, F., S. Vannitsem, and A. Barbosa (1998), Modeling of rainfall time series using two-state renewal processes and multifractals, *J. Geophys. Res.*, *103*(D18), 23,181–23,193.

Schoof, J. T., and S. Pryor (2001), Downscaling temperature and precipitation: A comparison of regression-based methods and artificial neural networks, *Int. J. Climatol.*, *21*(7), 773–790.

Seed, A. (2003), A dynamic and spatial scaling approach to advection forecasting., *J. Appl. Meteor.*, *42*(3).

Seed, A., C. Draper, R. Srikanthan, and M. Menabde (2000), A multiplicative broken-line model for time series of mean areal rainfall, *Water Resour. Res.*, *36*(8), 2395–2399.

Seed, A., P. Jordan, C. Pierce, M. Leonard, R. Nathan, E. Kordomenidi, et al. (2014), Stochastic simulation of space-time rainfall patterns for the brisbane river catchment, in *Hydrology and Water Resources Symposium*, Engineers Australia.

Seed, A. W., R. Srikanthan, and M. Menabde (1999), A space and time model for design storm rainfall, *J. Geophys. Res.*, *104*(D24), 31,623–31,630.

Seed, A. W., C. E. Pierce, and K. Norman (2013), Formulation and evaluation of a scale decomposition-based stochastic precipitation nowcast scheme, *Water Resour. Res.*, *49*(10), 6624–6641.

Srikanthan, R., and G. G. Pegram (2009), A nested multisite daily rainfall stochastic generation model, *J. Hydrol.*, *371*(1-4), 142–153.

Steinschneider, S., and C. Brown (2013), A semiparametric multivariate, multisite weather generator with low-frequency variability for use in climate risk assessments, *Water Resour. Res.*, *49*(11), 7205–7220.

Sun, Y., S. Solomon, A. Dai, and R. W. Portmann (2006), How often does it rain?, *J. Climate*, *19*(6), 916–934.

Timbal, B., A. Dufour, and B. McAvaney (2003), An estimate of future climate change for western France using a statistical downscaling technique, *Climate Dyn.*, *20*(7-8), 807–823.

Veneziano, D., R. L. Bras, and J. D. Niemann (1996), Nonlinearity and self-similarity of rainfall in time and a stochastic model, *J. Geophys. Res.*, *101*(D21), 26,371–26,392.

Venugopal, V., E. Foufoula-Georgiou, and V. Sapozhnikov (1999), A space-time downscaling model for rainfall, *J. Geophys. Res.*, *104*(D16), 19,705–19,721.

von Storch, H., E. Zorita, and U. Cubasch (1993), Downscaling of global climate change estimates to regional scales: An application to Iberian rainfall in wintertime, *J. Climate*, *6*(6), 1161–1171.

Vrac, M., M. Stein, and K. Hayhoe (2007), Statistical downscaling of precipitation through nonhomogeneous stochastic weather typing, *Climate Res.*, *34*(3), 169–184.

Waymire, E. (1985), Scaling limits and self-similarity in precipitation fields, *Water Resour. Res.*, *21*(8), 1271–1281.

Whitehead, P., R. Wilby, R. Battarbee, M. Kernan, and A. J. Wade (2009), A review of the potential impacts of climate change on surface water quality, *Hydrolog. Sci. J.*, *54*(1), 101–123.

Wilby, R. L., and T. Wigley (1997), Downscaling general circulation model output: A review of methods and limitations, *Prog. Phys. Geogr.*, *21*(4), 530–548.

Wilks, D. S. (1999), Multisite downscaling of daily precipitation with a stochastic weather generator, *Climate Res.*, *11*(2), 125–136.

Willems, P., K. Arnbjerg-Nielsen, J. Olsson, and V. Nguyen (2012), Climate change impact assessment on urban rainfall extremes and urban drainage: Methods and shortcomings, *Atmos. Res.*, *103*, 106–118.

Wong, T., and R. R. Brown (2009), The water sensitive city: Principles for practice, *Wat. Sci. Tech.*, *60*(3), 673–682.

Zhang, K., D. Manuelpillai, B. Raut, A. Deletic, and P. M. Bach (2019), Evaluating the reliability of stormwater treatment systems under various future climate conditions, *J. Hydrol.*, *568*, 57–66.

Zorita, E., and H. Von Storch (1999), The analog method as a simple statistical downscaling technique: comparison with more complicated methods, *J. Climate*, *12*(8), 2474–2489.